Inorg. Chem. **2008**, *47*, 11930−11941

Structures and Physical Properties of Rare-Earth Zinc Antimonides $Pr_6Zn_{1+x}Sb_{14+y}$ and $RE_6Zn_{1+x}Sb_{14}$ (RE = Sm, Gd−Ho)

Yi Liu,[†,‡] Ling Chen,[†,§] Long-Hua Li,[†] and Li-Ming Wu*[,†]

State Key Laboratory of Structural Chemistry, Fujian Institute of Research on the Structure of Matter, Chinese Academy of Sciences, Fuzhou, Fujian 350002, People's Republic of China, Graduate School of the Chinese Academy of Sciences, Beijing 100039, People's Republic of China, and State Key Laboratory for Physical Chemistry of Solid Surfaces, Xiamen University, Xiamen 361005, People's Republic of China

Oksana Ya. Zelinska[⊥,¶] and Arthur Mar*[,⊥]

Department of Chemistry, University of Alberta, Edmonton, Alberta, Canada T6G 2G2, and Department of Inorganic Chemistry, Ivan Franko National University of Lviv, 79005 Lviv, Ukraine

Received March 24, 2008

A new series of isostructural ternary rare-earth zinc antimonides $RE_6Zn_{1+x}Sb_{14+y}$ (RE = Pr, Sm, Gd−Ho) has been obtained by direct reaction of the elements at 1050−1100 °C. Single-crystal X-ray diffraction studies revealed that these compounds adopt an orthorhombic structure type (space group *Immm* (no. 71), $Z = 2$, $a = 4.28$−4.11 Å, $b = 15.15$−14.73 Å, $c = 19.13$−18.56 Å in the progression from RE = Pr to Ho) that may be regarded as stuffed variants of a $(U_{0.5}Ho_{0.5})_3Sb_7$-type host structure. Columns of face-sharing RE_6 trigonal prisms, centered by Sb atoms, occupy channels defined by an extensive polyanionic Sb network. This network is constructed from three-atom-wide and four-atom-wide Sb strips, the latter being linked together by single Sb atoms in $RE_6Zn_{1+x}Sb_{14}$ (RE = Sm, Gd−Ho; $y = 0$), but also by additional Sb−Sb pairs in a disordered fashion in $Pr_6Zn_{1+x}Sb_{14+y}$ ($y = \sim 0.6$). Interstitial Zn atoms then partially fill tetrahedral sites (occupancy of 0.5−0.7) and, to a lesser extent, square pyramidal sites (occupancy of 0.04−0.12), accounting for the observed nonstoichiometry with variable x. Except for the Gd member, these compounds undergo antiferromagnetic ordering below $T_N < 9$ K, with the magnetic susceptibilities of the Tb, Dy, and Ho members following the Curie−Weiss law above T_N. For the Ho member, the thermal conductivities are low and the Seebeck coefficients are small and positive, implying p-type character consistent with the occurrence of partial Zn occupancies. At low temperatures (down to 5 K), electrical resistivity measurements for the Tb, Dy, and Ho members indicated metallic behavior, which persists at high temperatures (up to 560 K) for the Ho member. Band structure calculations on an idealized "$Gd_6Zn_2Sb_{14}$" model revealed the existence of a pseudogap near the Fermi level.

Introduction

Ternary rare-earth antimonides *RE*-*M*-Sb, where *M* is a transition or post-transition metal, continue to attract growing interest because of their diverse structural chemistry and their potentially useful physical properties.[1,2] The Sb-rich phases exhibit various polyanionic Sb-based substructures made up of low-dimensional units such as clusters, chains, nets, and rings, with a wide range of Sb−Sb bonding interac-

* To whom correspondence should be addressed. E-mail: liming_wu@fjirsm.ac.cn (L.M.W.), arthur.mar@ualberta.ca (A.M.).
† Fujian Institute of Research on the Structure of Matter, CAS.
‡ Graduate School of the Chinese Academy of Sciences.
§ State Key Laboratory for Physical Chemistry of Solid Surfaces.
⊥ University of Alberta.
¶ Ivan Franko National University of Lviv.

(1) Sologub, O. L.; Salamakha, P. S. In *Handbook on the Physics and Chemistry of Rare Earths*; Gschneidner, K. A., Jr., Bünzli J.-C. G.; Pecharsky, V. K., Eds.; Elsevier: Amsterdam, 2003; Vol. *33*, pp 35−146.
(2) Mills, A. M.; Lam, R.; Ferguson, M. J.; Deakin, L.; Mar, A. *Coord. Chem. Rev.* **2002**, *233*−*234*, 207–222.

10.1021/ic800524d CCC: $40.75
Published on Web 11/11/2008

tions.[3−5] Although the presence of heavy elements leads to severe X-ray absorption problems and the complexity of the structures, marked by site disorder and partial occupancies, poses significant crystallographic challenges, these are the very features that are desirable in thermoelectric materials, such as found in the rare-earth-filled skutterudites, REM_4Sb_{12}.[6] The interplay of localized f electrons (from a *RE* component) and more delocalized d electrons (from a transition-metal component) frequently leads to interesting magnetic properties such as Kondo lattice behavior (e.g., $CeNiSb_3$)[7,8] and colossal magnetoresistance (e.g., $Eu_{14}MnSb_{11}$).[9] In some cases, the coexistence of localized electronic states, arising from discrete molecular-like units, with delocalized states, arising from the Sb substructures, has been proposed to account for the occurrence of superconductivity, as in $La_{13}Ga_8Sb_{21}$.[10]

The *RE*−Zn−Sb system typifies this diversity of structures and properties. The ternary phases known to date in this system are $Yb_{14}ZnSb_{11}$,[11−14] $Yb_9Zn_{4+x}Sb_9$,[15] $REZn_2Sb_2$ (*RE* = Eu, Yb),[16−22] $REZn_{1-x}Sb_2$ (*RE* = La−Nd, Sm, Gd, Tb),[23−29] and RE_6ZnSb_{15} (*RE* = La−Nd, Sm, Gd),[30] the latter two possessing extended polyanionic Sb substructures. Among these, $Yb_{14}ZnSb_{11}$ has been investigated for its thermoelectric properties,[13,14] and $YbZn_2Sb_2$ and $CeZn_{1-x}Sb_2$ exhibit Kondo lattice behavior.[22,28] The RE_6ZnSb_{15} series is especially interesting because it and its Mn and Cu analogues have been the subject of detailed theoretical study in which a "retrotheoretical" approach is applied to understand the complex Sb substructures.[3,4,31] Moreover, La_6ZnSb_{15} has recently been found to be a type II superconductor (T_c = 3.7 K).[32] Although a full single-crystal X-ray diffraction study was performed on La_6ZnSb_{15}, only cell parameters were obtained for the remaining RE_6ZnSb_{15} members, which were assumed to be isostructural.[30] One of the unusual features in the structure of La_6ZnSb_{15} is the presence of a short Sb−Sb bond (2.831(2) Å) which links puckered Sb sheets together. If the atomic positions for the other RE_6ZnSb_{15} members are assumed to be the same as for La_6ZnSb_{15}, the attendant structural contraction upon substitution with smaller *RE* atoms eventually leads to distances for this Sb−Sb bond (from 2.791(2) Å for Ce_6ZnSb_{15} to 2.740(2) Å for Gd_6ZnSb_{15}) that would be unusually short for a single bond or imply the (unlikely) assignment of multiple bond character. Another ambiguity relates to the occupancy of an interstitial Zn site, which was fixed at 0.50 in La_6ZnSb_{15} and assumed to be the same for the other RE_6ZnSb_{15} members. These questions led us to re-examine this series and to extend the investigation to later *RE* elements, where no *RE*−Zn−Sb phases (except for those containing Yb) were known so far.

We report here the series of rare-earth zinc antimonides, $RE_6Zn_{1+x}Sb_{14+y}$ (*RE* = Pr, Sm, Gd−Ho) which is related to La_6ZnSb_{15} but is slightly antimony-poorer and contains two possible interstitial Zn sites. The transition from RE_6ZnSb_{15} (for early *RE*) to $RE_6Zn_{1+x}Sb_{14}$ (for late *RE*) was clarified by elucidating the structure of an intermediate member, $Pr_6Zn_{1+x}Sb_{14+y}$, showing that the Sb content gradually diminishes on proceeding to a later *RE*. The potential of these compounds as magnetic or thermoelectric materials was assessed by measuring their magnetic and transport properties (including electrical resistivity, Seebeck coefficient, and thermal conductivity) and relating them to the calculated electronic structure.

Experimental Section

Synthesis. Starting materials were either powders or pieces of rare-earth elements (Pr, Sm, Gd, Tb, Dy, Ho; 99.9% or better, Alfa-Aesar or Huhhot Jinrui Rare Earth Co. Ltd.), zinc (99.95% or better, Spex or Alfa-Aesar), and antimony (99.99%, Alfa-Aesar). All manipulations were performed in a N_2- or Ar-filled glovebox, although the title compounds were subsequently found to be stable

(3) Papoian, G. A.; Hoffmann, R. *Angew. Chem., Int. Ed.* **2000**, *39*, 2408–2448.
(4) Papoian, G.; Hoffmann, R. *J. Am. Chem. Soc.* **2001**, *123*, 6600–6608.
(5) Kleinke, H. *Chem. Soc. Rev.* **2000**, *29*, 411–418.
(6) Nolas, G. S.; Morelli, D. T.; Tritt, T. M. *Annu. Rev. Mater. Sci.* **1999**, *29*, 89–116.
(7) Macaluso, R. T.; Wells, D. M.; Sykora, R. E.; Albrecht-Schmitt, T. E.; Mar, A.; Nakatsuji, S.; Lee, H.; Fisk, Z.; Chan, J. Y. *J. Solid State Chem.* **2004**, *177*, 293–298.
(8) Thomas, E. L.; Gautreaux, D. P.; Lee, H.-O.; Fisk, Z.; Chan, J. Y. *Inorg. Chem.* **2007**, *46*, 3010–3016.
(9) Chan, J. Y.; Kauzlarich, S. M.; Klavins, P.; Shelton, R. N.; Webb, D. J. *Chem. Mater.* **1997**, *9*, 3132–3135.
(10) Mills, A. M.; Deakin, L.; Mar, A. *Chem. Mater.* **2001**, *13*, 1778–1788.
(11) Fisher, I. R.; Bud'ko, S. L.; Song, C.; Canfield, P. C.; Ozawa, T. C.; Kauzlarich, S. M. *Phys. Rev. Lett.* **2000**, *85*, 1120–1123.
(12) Holm, A. P.; Ozawa, T. C.; Kauzlarich, S. M.; Morton, S. A.; Waddill, G. D.; Tobin, J. G. *J. Solid State Chem.* **2005**, *178*, 262–269.
(13) Ribeiro, R. A.; Hadano, Y.; Narazu, S.; Suekuni, K.; Avila, M. A.; Takabatake, T. *J. Phys.: Condens. Matter* **2007**, *19*, 376211/1–376211/6.
(14) Brown, S. R.; Toberer, E. S.; Ikeda, T.; Cox, C. A.; Gascoin, F.; Kauzlarich, S. M.; Snyder, J. G. *Chem. Mater.* **2008**, *20*, 3412–3419.
(15) Bobev, S.; Thompson, J. D.; Sarrao, J. L.; Olmstead, M. M.; Hope, H.; Kauzlarich, S. M. *Inorg. Chem.* **2004**, *43*, 5044–5052.
(16) Klüfers, P.; Neumann, H.; Mewis, A.; Schuster, H.-U. *Z. Naturforsch. B: Anorg. Chem. Org. Chem.* **1981**, *35*, 1317–1318.
(17) Zwiener, G.; Neumann, H.; Schuster, H.-U. *Z. Naturforsch. B: Anorg. Chem. Org. Chem.* **1981**, *36*, 1195–1197.
(18) Pfleiderer, C.; Vollmer, R.; Uhlarz, M.; Faisst, A.; von Löhneysen, H.; Nateprov, A. *Physica B* **2002**, *312*−*313*, 352–353.
(19) Gascoin, F.; Ottensmann, S.; Stark, S.; Haïle, S. M.; Snyder, J. G. *Adv. Funct. Mater.* **2005**, *15*, 1860–1864.
(20) Weber, F.; Cosceev, A.; Nateprov, A.; Pfleiderer, C.; Faisst, A.; Uhlarz, M.; von Löhneysen, H. *Physica B* **2005**, *359*−*361*, 226–228.
(21) Weber, F.; Cosceev, A.; Drobnik, S.; Faisst, A.; Grube, K.; Nateprov, A.; Pfleiderer, C.; Uhlarz, M.; von Löhneysen, H. *Phys. Rev. B* **2006**, *73*, 014427/1−014427/7.
(22) Zelinska, O. Ya.; Tkachuk, A. V.; Grosvenor, A. P.; Mar, A. *Chem. Met. Alloys.* **2008**, *1*, 204–209.
(23) Cordier, G.; Schäfer, H.; Woll, P. *Z. Naturforsch. B: Anorg. Chem. Org. Chem.* **1985**, *40*, 1097–1099.
(24) Sologub, O.; Hiebl, K.; Rogl, P.; Bodak, O. *J. Alloys Compd.* **1995**, *227*, 40–43.
(25) Flandorfer, H.; Sologub, O.; Godart, C.; Hiebl, K.; Leithe-Jasper, A.; Rogl, P.; Noël, H. *Solid State Commun.* **1996**, *97*, 561–565.
(26) Wollesen, P.; Jeitschko, W.; Brylak, M.; Dietrich, L. *J. Alloys Compd.* **1996**, *245*, L5–L8.
(27) Salamakha, L. P.; Mudryi, S. I. *J. Alloys Compd.* **2003**, *359*, 139–142.
(28) Park, T.; Sidorov, V. A.; Lee, H.; Fisk, Z.; Thompson, J. D. *Phys. Rev. B* **2005**, *72*, 060410/1–060410/4.
(29) Zelinska, O. Ya.; Mar, A. *J. Solid State Chem.* **2006**, *179*, 3776–3783.
(30) Sologub, O.; Vybornov, M.; Rogl, P.; Hiebl, K.; Cordier, G.; Woll, P. *J. Solid State Chem.* **1996**, *122*, 266–272.
(31) Papoian, G.; Hoffmann, R. *J. Solid State Chem.* **1998**, *139*, 8–21.
(32) Wakeshima, M.; Sakai, C.; Hinatsu, Y. *J. Phys.: Condens. Matter* **2007**, *19*, 016218/1−016218/10.

Table 1. Crystallographic Data for $RE_6Zn_{1+x}Sb_{14+y}$ (RE = Pr, Sm, Gd−Ho)

formula	$Pr_6Zn_{1.22(4)}Sb_{14.59(3)}$	$Sm_6Zn_{1.52(5)}Sb_{14.02(4)}$	$Gd_6Zn_{1.49(3)}Sb_{14}$	$Tb_6Zn_{1.41(3)}Sb_{14}$	$Dy_6Zn_{1.38(3)}Sb_{14}$	$Ho_6Zn_{1.13(3)}Sb_{14}$
formula mass (amu)	2700.61	2705.96	2745.40	2750.52	2770.04	2768.27
space group	*Immm* (No. 71)	*Immm* (No. 71)	*Immm* (No. 71)	*Immm* (No. 71)	*Immm* (No. 71)	*Immm* (No. 71)
a (Å)	4.2764(4)	4.184(1)	4.1569(4)	4.1426(2)	4.1373(4)	4.1050(4)
b (Å)	15.148(1)	15.039(5)	14.971(2)	14.874(1)	14.802(1)	14.725(2)
c (Å)	19.127(2)	18.832(6)	18.744(2)	18.662(1)	18.611(2)	18.562(2)
V (Å^3)	1239.1(2)	1184.9(6)	1166.5(2)	1149.9(1)	1139.7(2)	1122.0(2)
Z	2	2	2	2	2	2
T (°C)	22	20	22	22	22	22
λ (Å)	0.71073	0.71073	0.71073	0.71073	0.71073	0.71073
ρ_{calcd} (g cm^{-3})	7.239	7.584	7.816	7.944	8.072	8.194
μ(Mo $K\alpha$) (cm^{-1})	282.6	317.3	341.6	357.2	370.6	385.6
$R(F)$ for $F_o^2 > 2\sigma(F_o^2)^a$	0.041	0.034	0.032	0.032	0.032	0.035
$R_w(F_o^2)^b$	0.095	0.082	0.072	0.071	0.079	0.076

^{a} $R(F) = \sum||F_o| - |F_c||/\sum|F_o|$. ^{b} $R_w(F_o^2) = [\sum[w(F_o^2 - F_c^2)^2]/\sum wF_o^4]^{1/2}$; $w^{-1} = [\sigma^2(F_o^2) + (Ap)^2 + Bp]$ where $p = [\max(F_o^2,0) + 2F_c^2]/3$.

in air for up to 2 months. Reactions were performed by direct combination of the elements in appropriate proportions, sealed within fused-silica tubes under vacuum. Products were characterized by powder X-ray diffraction (on an Inel powder diffractometer equipped with a CPS 120 detector or a Rigaku D/MAX 2500 powder diffractometer, both with Cu Kα radiation) and energy-dispersive X-ray (EDX) analysis (on a Hitachi S-2700 scanning electron microscope or a JEOL JSM6700F field-emission scanning electron microscope).

Samples of $RE_6Zn_{1+x}Sb_{14+y}$ (RE = Pr, Sm, Gd−Ho) were first identified as byproducts in the synthesis at 1050 °C of $RE Zn_{1-x}Sb_2$, which forms with ease for the early RE (La−Nd, Sm) and with greater difficulty for the later RE metals (Gd, Tb).[29] These two phases are readily distinguished by the needle- or block-like habit of $RE_6Zn_{1+x}Sb_{14+y}$ crystals versus the plate-like habit of $RE Zn_{1-x}Sb_2$ crystals. Moreover, EDX analyses revealed consistently lower Zn content in the block-shaped crystals (27−33% RE, 6−8% Zn, 61−65% Sb) than in the plate-shaped crystals (27−30% RE, 19−23% Zn, 51−53% Sb). However, the uncertainties inherent in semiquantitative EDX analysis do not permit sufficient discrimination among the various possible ideal compositions, "RE_6ZnSb_{14}" (29% RE, 5% Zn, 67% Sb), "$RE_6Zn_2Sb_{14}$" (27% RE, 9% Zn, 64% Sb), or "RE_6ZnSb_{15}" (27% RE, 5% Zn, 68% Sb), for the block-shaped crystals. Potential impurities of silicon and oxygen (from the silica tube) were not detected. Ultimate composition was established from structural refinements based on the X-ray diffraction data.

Synthesis of $RE_6Zn_{1+x}Sb_{14}$ (RE = Sm, Gd−Ho) was optimized with use of the loading composition "$RE_6Zn_2Sb_{14}$". Reactants were placed within an inner alumina crucible or a thinner fused-silica tube, jacketed by an outer fused-silica tube, to minimize adventitious reactions with the container. Flame-sealing the tube during evacuation reduces the possibility of hydrogen incorporation. A successful temperature profile entails heating at 25 °C/h to 1100 °C, annealing at that temperature for 96 h, slowly cooling at 4 °C/h to 200 °C, and radiative cooling to ambient temperature. Powder X-ray diffraction patterns of the resulting products match well with those simulated from the single-crystal X-ray structures.

In the course of the crystallographic investigations, questions arose about the nature of the related RE_6ZnSb_{15} (RE = La−Nd, Sm, Gd) compounds that had been reported previously.[30] As an intermediate candidate for further study, the Pr member was chosen, for which crystals were obtained through use of excess Sb as a self-flux with the loading composition "$PrZnSb_{10}$". Heating at 1050 °C for 3 h, cooling slowly at 3.5 °C/h to 700 °C, and centrifuging the tube to remove the flux through a glass-wool filter afforded crystals of $Pr_6Zn_{1+x}Sb_{14+y}$.

Structure Determination. Single-crystal X-ray diffraction data were collected on a Bruker Platform/SMART 1000, a Rigaku Mercury, or a Rigaku Saturn70 CCD diffractometer at room temperature (20−22 °C) using ω scans. Structure solution and refinement were carried out with use of the SHELXTL (version 6.12) program package.[33] Face-indexed numerical absorption corrections were applied. Crystal data and further details of the data collection are given in Table 1. For all compounds, intensity statistics (values of $\langle|E|^2-1\rangle$ ranged from 1.02 to 1.09) favored the centrosymmetric orthorhombic space group *Immm*. From direct methods, the initial atomic positions of the RE and most Sb atoms were readily located, which were then standardized relative to $(U_{0.5}Ho_{0.5})_3Sb_7$,[34] the host structure for these and related compounds.

For $RE_6Zn_{1+x}Sb_{14}$ (RE = Sm, Gd−Ho), the difference map revealed prominent electron density at Wyckoff position 4*h* (0, ~0.26, 1/2) corresponding to an interstitial Zn site, labeled as Zn2, with tetrahedral coordination geometry. Reasonable displacement parameters for this site could only be achieved through partial Zn occupancy, which converged to values ranging from 0.5 to 0.7, depending on the RE member. Another interstitial Zn site with square pyramidal geometry, labeled as Zn1, was also located at Wyckoff position 4*j* (1/2, 0, ~0.44) but with a considerably lower occupancy (<0.1). Moreover, the Sb5 atoms occupy two sets of closely spaced but distinct sites: Sb5a at 2*c* (1/2, 1/2, 0) and Sb5b at 4*f* (~0.40, 1/2, 0). The Zn1, Sb5a, and Sb5b sites are correlated and must be partially occupied to preclude chemically unreasonable short distances to symmetry-equivalent positions. For example, in the succession of sites Sb5b-Sb5a-Sb5b′ (at positions ~0.40, 1/2, 0; 1/2, 1/2, 0; ~0.60, 1/2, 0, respectively, which are separated at increments of ~0.4 Å), the condition that must be satisfied is $k_{Sb5a} + 2k_{Sb5b} = 1$, where k is the occupancy. With this restraint applied in the refinements, the occupancies converged to 0.42−0.25 for Sb5a and 0.29−0.38 for Sb5b. Another condition is that Zn atoms cannot simultaneously occupy two square pyramidal Zn1 sites located on opposite sides of a common square face, to preclude impossibly short Zn1−Zn1′ distances of ~2.3 Å. When freely refined, the Zn1 occupancy converged to ~0.1, which is sufficiently low to satisfy this condition without the need to apply further restraints. (The tetrahedral Zn2 sites do not suffer from any such restrictions.) All remaining atoms were confirmed, in separate refinements, to be fully occupied.

For $Pr_6Zn_{1+x}Sb_{14+y}$, similar interstitial square pyramidal Zn1 and tetrahedral Zn2 sites were located in the difference electron density map, and treated as above. However, there are now two sets of split Sb sites: Sb5a/Sb5b and Sb6a/Sb6b. The separation within a

(33) Sheldrick, G. M. *SHELXTL*, version 6.12; Bruker AXS Inc.: Madison, WI, 2001.
(34) Schmidt, T.; Jeitschko, W. *Inorg. Chem.* **2001**, *40*, 6356–6361.

succession of split Sb6b-Sb6a-Sb6b sites is considerably greater, at increments of 1.4 Å, such that a simple disorder can be envisioned between two models of the local structure: a single Sb6a atom versus a Sb6b-Sb6b dumbbell (with a 2.8 Å bond). With the restraint $k_{Sb6a} + k_{Sb6b} = 1$ applied in the refinement, the occupancies converged to 0.35 for Sb6a and 0.61 for Sb6b. Subsequent re-examination of the structure of the Sm member revealed that split Sb6a/Sb6b sites can also be modeled; however, the Sb6b-Sb6b′ distance here is too short (2.56(4) Å) to imply the presence of a dumbbell so that the restraint $k_{Sb6a} + 2k_{Sb6b} = 1$ must be applied instead. The refined occupancies of 0.87 for Sb6a and 0.08 for Sb6b, corresponding to the formula $Sm_6Zn_{1.52(5)}Sb_{14.02(4)}$, suggest a local structure that is essentially the same as for the remaining *RE* members ($RE_6Zn_{1+x}Sb_{14}$) but with an occasional asymmetric disposition of this Sb atom.

Some of the lower symmetry space groups (*Imm*2 and its permutations, *I*222, $I2_12_12_1$) were considered, but these did not support ordered models similar to that found for La_6ZnSb_{15}, where the mirror plane normal to the short 4 Å axis is absent and three-atom-wide Sb ribbons are distorted exclusively in one direction. Final refinements included anisotropic displacement parameters for all atoms except those in closely spaced split sites (Zn1, Sb5a/5b, Sb6a/6b), where only isotropic displacement parameters were used. Final values of the positional and displacement parameters are given in Table 2. Selected interatomic distances are listed in Table 3. Further data, in the form of crystallographic information files (CIFs), are available as Supporting Information or may be obtained from Fachinformationszentrum Karlsruhe, Abt. PROKA, 76344 Eggenstein-Leopoldshafen, Germany (No. CSD-419984 (Pr6Zn1.2Sb14.6), 419983 (Sm6Zn1.5Sb14.0), 419987 (Gd6Zn1.5Sb14), 419981 (Tb6Zn1.4Sb14), 419989 (Dy6Zn1.4Sb14), 419985 (Ho6Zn1.1Sb14)). Except for the Sm member, the crystallographic data chosen for presentation here are from the Alberta group.

Property Measurements. Magnetic susceptibility measurements were made on a Quantum Design PPMS-9T magnetometer between 2 and 300 K. Polycrystalline samples of $RE_6Zn_{1+x}Sb_{14}$ (*RE* = Sm, Gd−Ho), prepared by grinding to fine powders to minimize anisotropic effects, were loaded into gelatin capsules and cooled in a constant magnetic field of 5000 Oe. Susceptibility values were corrected for contributions from the container and from ion-core diamagnetism.

Low-temperature (2−300 K) electrical resistivity measurements were made on single crystals of $RE_6Zn_{1+x}Sb_{14}$ (*RE* = Tb−Ho), which were sufficiently large (0.3 to 0.4 mm in length) to apply standard four-probe methods on a Quantum Design PPMS system equipped with an ac transport controller (Model 7100). The current was 100 μA and the frequency was 16 Hz.

High-temperature (300−700 K) electrical and thermal transport measurements were made on a sample of nominal composition $Ho_6Zn_{1.35}Sb_{14}$, prepared by reaction of the elements in the ratio Ho/Zn/Sb = 6:1.35:14 according to the optimized conditions described earlier. (This composition was chosen based on the formula obtained from a single-crystal X-ray structure refinement separate from that reported here (vide infra).) The powder sample, which was uniform in color and morphology and contained no other detectable phases as judged by its X-ray diffraction pattern, was cold-pressed into a 3.1 × 3.1 × 9.1 mm bar-shaped pellet whose density attains ∼80% of the theoretical value calculated from the formula refined from the single-crystal X-ray data. Measurements were made on an ULVAC-RIKO ZEM-3 thermoelectrics evaluation instrument. Electrical conductivity was measured by four-probe methods under flowing Ar atmosphere, and Seebeck coefficients were measured three times under different temperature gradients (from 20 to 40 K) at each temperature step. The total thermal conductivity (κ) was derived from the relationship $\kappa = \rho\lambda C_p$, where ρ is the density of the pellet, λ is the thermal diffusivity, and C_p is the specific heat capacity. The thermal diffusivity was measured by the flash-diffusivity-heat-capacity method on a NETZSCH LFA 457 MicroFlash instrument, whereby the front face of a disk-shaped specimen (∅10 × 1.5 mm) is heated by a short energy pulse generated by a laser beam. The thermal diffusivity was determined by the shape of the temperature rise on the rear sample surface versus time using an infrared detector.

Except for the single-crystal electrical resistivity measurements, all physical properties were determined in the Fujian group and refer to samples that are slightly Zn-richer than those used for structure determination.

Band Structure. Ab initio band structure and total energy calculations were carried out for a hypothetical "$Gd_6Zn_2Sb_{14}$" model, in space group *Immm*, where the tetrahedral Zn2 site is assumed to be fully occupied and the square pyramidal Zn1 site is empty. The valence electron configurations are: Gd, [Xe] $4f^7\ 5d^1\ 6s^2$; Zn, [Ar] $3d^{10}\ 4s^2$; and Sb, [Kr] $4d^{10}\ 5s^2\ 5p^3$. A full-potential linear augmented plane wave method was applied within density functional theory (DFT),[35−37] with augmented plane waves and local orbitals (APW+lo), as implemented in the WIEN2k package.[38] The GGA from Perdew et al. was used for the exchange-correlation potential.[39] Full relativistic effects were taken for the core states and scalar relativistic approximations were used for the valence states, with spin−orbit coupling neglected. The muffin-tin radii were fixed to 2.50, 2.20, and 2.32 au for Gd, Zn, and Sb atoms, respectively. The basis function was expanded up to $R_{mt} \times K_{max} = 8.0$. The maximum value of partial waves inside the atomic sphere was $l_{max} = 10$ and $G_{max} = 14$ in the charge density Fourier expansion. The Brillouin zone integration was performed on a 4 × 4 × 4 Monkhorst−Park mesh, which corresponds to 64 *k* points. The density of states (DOS) was calculated with the modified tetrahedron method.[40] Self-consistent iterations were performed until the total energy converged to less than 0.0001 Ry.

Results and Discussion

Phase Composition. The most Sb-rich phase previously found within the ternary *RE*−Zn−Sb systems was RE_6ZnSb_{15} (*RE* = La−Nd, Sm, Gd), prepared by reaction of the elements at 600 °C.[30] Only the La member was fully characterized by single-crystal X-ray diffraction. We report here an apparently new phase with a slightly different composition, $RE_6Zn_{1+x}Sb_{14+y}$ (*RE* = Pr, Sm, Gd−Ho), prepared by reaction of the elements at 1050−1100 °C. The overlap of some of the *RE* members (*RE* = Pr, Sm, Gd) might, at first thought, be attributed to a distinction between a low- versus a high-temperature phase. However, inspection of the cell parameters (Supporting Information, Table S1) provided the first indication that these may, in fact, be the

(35) Yu, R.; Singh, D.; Krakauer, H. *Phys. Rev. B* **1991**, *43*, 6411–6422.
(36) Wimmer, E.; Krakauer, H.; Weinert, M.; Freeman, A. J. *Phys. Rev. B* **1981**, *24*, 864–875.
(37) Matthiess, L. F.; Hamann, D. R. *Phys. Rev. B* **1986**, *33*, 823–840.
(38) Blaha, P.; Schwarz, K.; Madsen, G. K. H.; Kvasnicka, D.; Luitz, J. *WIEN2k, An Augmented Plane Wave + Local Orbitals Program for Calculating Crystal Properties*; Karlheinz Schwarz, Techn. Universität Wien: Vienna, Austria, 2001.
(39) Perdew, J. P.; Burke, K.; Ernzerhof, M. *Phys. Rev. Lett.* **1996**, *77*, 3865–3868.
(40) Blöchl, P. E.; Jepsen, O.; Andersen, O. K. *Phys. Rev. B* **1994**, *49*, 16223–16233.

Table 2. Atomic Coordinates and Equivalent Isotropic Displacement Parameters for $RE_6Zn_{1+x}Sb_{14+y}$ (RE = Pr, Sm, Gd−Ho)

atom	Wyckoff position	occupancy	x	y	z	U_{iso}*/U_{eq} (Å^2)[a]
			$Pr_6Zn_{1.22(4)}Sb_{14.59(3)}$			
Pr1	8*l*	1	0	0.13870(4)	0.36484(3)	0.0081(2)
Pr2	4*i*	1	0	0	0.17447(5)	0.0094(2)
Zn1	4*j*	0.124(9)	1/2	0	0.4366(8)	0.009(4)*
Zn2	4*h*	0.482(10)	0	0.2603(3)	1/2	0.014(1)
Sb1	8*l*	1	0	0.21353(5)	0.20025(4)	0.0104(2)
Sb2	8*l*	1	0	0.35989(6)	0.39501(5)	0.0183(2)
Sb3	4*j*	1	1/2	0	0.30054(6)	0.0087(2)
Sb4	4*g*	1	0	0.34570(7)	0	0.0100(2)
Sb5a	2*c*	0.152(9)	1/2	1/2	0	0.0100(6)*
Sb5b	4*f*	0.428(5)	0.3879(9)	1/2	0	0.0100(6)*
Sb6a	2*a*	0.350(5)	0	0	0	0.0262(6)*
Sb6b	4*g*	0.614(5)	0	0.0923(2)	0	0.0262(6)*
			$Sm_6Zn_{1.52(5)}Sb_{14.02(4)}$			
Sm1	8*l*	1	0	0.13848(4)	0.36405(3)	0.0058(2)
Sm2	4*i*	1	0	0	0.17577(5)	0.0079(2)
Zn1	4*j*	0.086(12)	1/2	0	0.439(1)	0.018(10)*
Zn2	4*h*	0.674(11)	0	0.2623(2)	1/2	0.0105(11)
Sb1	8*l*	1	0	0.21183(5)	0.19784(4)	0.0074(2)
Sb2	8*l*	1	0	0.36688(7)	0.39839(6)	0.0182(3)
Sb3	4*j*	1	1/2	0	0.30171(6)	0.0060(3)
Sb4	4*g*	1	0	0.34750(8)	0	0.0090(3)
Sb5a	2*c*	0.414(12)	1/2	1/2	0	0.0071(7)*
Sb5b	4*f*	0.292(6)	0.392(2)	1/2	0	0.0071(7)*
Sb6a	2*a*	0.869(8)	0	0	0	0.0237(7)*
Sb6b	4*g*	0.077(4)	0	0.0849(14)	0	0.0237(7)*
			$Gd_6Zn_{1.49(3)}Sb_{14}$			
Gd1	8*l*	1	0	0.13837(3)	0.36367(2)	0.0085(1)
Gd2	4*i*	1	0	0	0.17666(3)	0.0103(1)
Zn1	4*j*	0.044(8)	1/2	0	0.4375(16)	0.006(8)*
Zn2	4*h*	0.701(9)	0	0.2618(2)	1/2	0.0153(7)
Sb1	8*l*	1	0	0.21125(4)	0.19734(3)	0.0097(1)
Sb2	8*l*	1	0	0.36847(5)	0.39879(4)	0.0209(2)
Sb3	4*j*	1	1/2	0	0.30222(4)	0.0084(2)
Sb4	4*g*	1	0	0.34779(6)	0	0.0121(2)
Sb5a	2*c*	0.415(7)	1/2	1/2	0	0.0087(4)*
Sb5b	4*f*	0.287(4)	0.3979(12)	1/2	0	0.0087(4)*
Sb6	2*a*	1	0	0	0	0.0281(4)
			$Tb_6Zn_{1.41(3)}Sb_{14}$			
Tb1	8*l*	1	0	0.13843(3)	0.36367(2)	0.0082(1)
Tb2	4*i*	1	0	0	0.17685(3)	0.0099(1)
Zn1	4*j*	0.048(8)	1/2	0	0.4372(16)	0.008(8)*
Zn2	4*h*	0.659(9)	0	0.2617(2)	1/2	0.0136(7)
Sb1	8*l*	1	0	0.21116(4)	0.19738(3)	0.0091(1)
Sb2	8*l*	1	0	0.36858(5)	0.39933(4)	0.0209(2)
Sb3	4*j*	1	1/2	0	0.30216(4)	0.0080(2)
Sb4	4*g*	1	0	0.34697(6)	0	0.0122(2)
Sb5a	2*c*	0.368(8)	1/2	1/2	0	0.0087(5)*
Sb5b	4*f*	0.312(4)	0.3992(12)	1/2	0	0.0087(5)*
Sb6	2*a*	1	0	0	0	0.0256(3)
			$Dy_6Zn_{1.38(3)}Sb_{14}$			
Dy1	8*l*	1	0	0.13854(2)	0.36352(2)	0.0117(1)
Dy2	4*i*	1	0	0	0.17667(3)	0.0137(1)
Zn1	4*j*	0.089(8)	1/2	0	0.4379(9)	0.018(5)*
Zn2	4*h*	0.603(8)	0	0.2615(2)	1/2	0.017(1)
Sb1	8*l*	1	0	0.21113(4)	0.19726(3)	0.0123(1)
Sb2	8*l*	1	0	0.36796(5)	0.40024(4)	0.0248(2)
Sb3	4*j*	1	1/2	0	0.30179(4)	0.0113(2)
Sb4	4*g*	1	0	0.34526(6)	0	0.0162(2)
Sb5a	2*c*	0.256(8)	1/2	1/2	0	0.0143(4)*
Sb5b	4*f*	0.375(5)	0.3956(10)	1/2	0	0.0143(4)*
Sb6	2*a*	1	0	0	0	0.0269(3)
			$Ho_6Zn_{1.13(3)}Sb_{14}$			
Ho1	8*l*	1	0	0.13835(3)	0.36396(2)	0.0104(1)
Ho2	4*i*	1	0	0	0.17708(4)	0.0122(2)
Zn1	4*j*	0.043(8)	1/2	0	0.442(3)	0.030(15)*
Zn2	4*h*	0.525(7)	0	0.2611(2)	1/2	0.014(1)
Sb1	8*l*	1	0	0.21101(4)	0.19730(4)	0.0111(2)
Sb2	8*l*	1	0	0.36693(6)	0.40163(5)	0.0242(2)
Sb3	4*j*	1	1/2	0	0.30210(5)	0.0100(2)
Sb4	4*g*	1	0	0.34562(7)	0	0.0146(2)
Sb5a	2*c*	0.25(2)	1/2	1/2	0	0.0111(5)*
Sb5b	4*f*	0.375(10)	0.4103(18)	1/2	0	0.0111(5)*
Sb6	2*a*	1	0	0	0	0.0267(4)

[a] U_{eq} is defined as one-third of the trace of the orthogonalized U_{ij} tensor. Values marked in asterisks refer to U_{iso}.

same phase. The unit cell volumes obtained from three independent laboratories are very similar (Figure 1). As revealed by the structural studies below, there is actually a gradual transition from RE_6ZnSb_{15} to $RE_6Zn_{1+x}Sb_{14}$ on progressing from the early to the late RE members, such that the common formulation $RE_6Zn_{1+x}Sb_{14+y}$ probably

Table 3. Selected Interatomic Distances (Å) in $RE_6Zn_{1+x}Sb_{14+y}$ (RE = Pr, Sm, Gd−Ho)[a]

	$Pr_6Zn_{1.22(4)}Sb_{14.59(3)}$	$Sm_6Zn_{1.52(5)}Sb_{14.02(4)}$	$Gd_6Zn_{1.49(3)}Sb_{14}$	$Tb_6Zn_{1.41(3)}Sb_{14}$	$Dy_6Zn_{1.38(3)}Sb_{14}$	$Ho_6Zn_{1.13(3)}Sb_{14}$
*RE*1−Sb3 (× 2)	3.2402(7)	3.1768(9)	3.1525(5)	3.1381(4)	3.1312(4)	3.1115(5)
*RE*1−Sb1 (× 2)	3.3366(8)	3.2867(10)	3.2705(6)	3.2548(5)	3.2418(5)	3.2290(6)
*RE*1−Sb4 (× 2)	3.3631(6)	3.3128(9)	3.3005(4)	3.2879(3)	3.2847(4)	3.2627(4)
*RE*1−Sb1	3.3461(10)	3.3188(14)	3.3031(8)	3.2864(7)	3.2755(7)	3.2734(9)
*RE*1−Sb5a	3.3312(7)	3.3002(10)	3.2897(5)	3.2730(4)	3.2645(4)	3.2445(5)
*RE*1−Sb5b	3.3655(9)	3.3308(15)	3.3169(8)	3.2995(8)	3.2930(7)	3.2653(10)
*RE*1−Sb2	3.4001(12)	3.4953(16)	3.5071(9)	3.4875(9)	3.4638(9)	3.4377(10)
*RE*1−Zn2	3.174(3)	3.166(2)	3.154(1)	3.136(2)	3.125(2)	3.106(2)
*RE*1−Zn1 (× 2)	3.297(7)	3.272(13)	3.245(13)	3.227(13)	3.225(8)	3.23(3)
*RE*2−Sb3 (× 2)	3.2229(11)	3.1624(13)	3.1399(8)	3.1238(8)	3.1148(7)	3.0981(9)
*RE*2−Sb1 (× 2)	3.2720(8)	3.2129(13)	3.1863(7)	3.1641(6)	3.1485(6)	3.1297(7)
*RE*2−Sb2 (× 4)	3.2928(8)	3.2148(11)	3.1933(7)	3.1831(7)	3.1856(7)	3.1918(8)
*RE*2−Sb6	3.3371(10) (−Sb6a)	3.3100(14) (−Sb6a)	3.3113(7)	3.3004(6)	3.2880(6)	3.2871(8)
	3.6183(13) (−Sb6b)	3.548(8) (−Sb6b)				
Zn1−Sb3	2.60(2)	2.59(3)	2.54(3)	2.52(3)	2.53(1)	2.59(6)
Zn1−Sb4 (× 2)	2.63(1)	2.56(1)	2.56(1)	2.56(1)	2.57(1)	2.52(2)
Zn1−Sb5b (× 2)	2.89(1)	2.79(1)	2.76(1)	2.75(1)	2.76(1)	2.65(2)
Zn2−Sb2 (× 2)	2.512(3)	2.477(2)	2.480(2)	2.461(2)	2.435(2)	2.400(2)
Zn2−Sb4 (× 2)	2.674(3)	2.665(2)	2.648(2)	2.628(2)	2.604(2)	2.585(2)
Sb1−Sb2 (× 2)	3.0214(9)	3.0102(11)	2.9984(7)	2.9924(7)	2.9903(7)	2.9837(8)
Sb1−Sb1 (× 2)	3.0683(12)	3.0908(13)	3.0926(9)	3.0793(9)	3.0753(8)	3.0592(10)
Sb4−Sb5b (× 2)	2.866(3)	2.820(5)	2.816(3)	2.813(3)	2.815(3)	2.829(4)
Sb4−Sb5a (× 2)	3.168(1)	3.104(1)	3.084(1)	3.078(1)	3.086(1)	3.063(8)
Sb4−Sb5b (× 2)	3.509(3)	3.424(6)	3.385(4)	3.373(4)	3.391(3)	3.321(5)
Sb2−Sb6 (× 2)	3.0214(9) (−Sb6b)	2.926(5) (−Sb6b)	3.4346(6)	3.4119(6)	3.3980(6)	3.3744(7)
	3.6207(8) (−Sb6a)	3.471(1) (−Sb6a)				
Sb6b−Sb6b	2.797(5)	[2.56(4)]				

[a] Zn1 and Zn2 are partially occupied, and Sb5a/Sb5b and Sb6a/Sb6b are split sites (see Table 2 for occupancies).

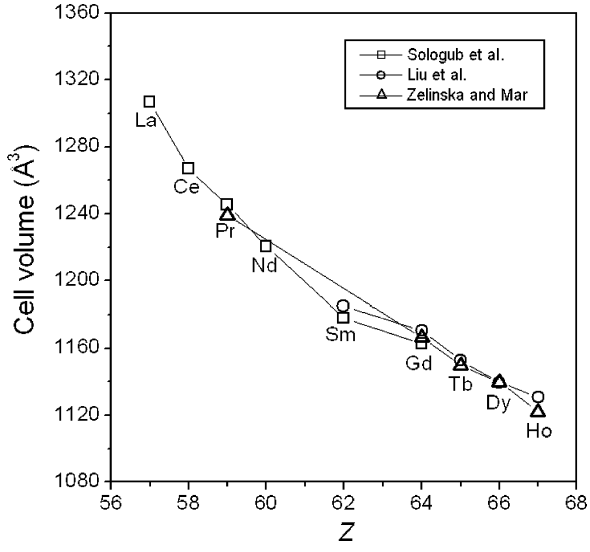

Figure 1. Cell volumes for nominal RE_6ZnSb_{15} (ref 30) and $RE_6Zn_{1+x}Sb_{14+y}$ compounds (this work).

best represents the continuum of phases for the entire *RE* series. Because the Zn atoms can be considered as stuffing a host structure, as discussed later, the alternative formula "$RE_6Zn_xSb_{14+y}$" is possible; however, here we wish to emphasize the relationship to the previously known RE_6ZnSb_{15} compounds.

These results do not rule out the possibility that the formation of $RE_6Zn_{1+x}Sb_{14+y}$ depends strongly on the temperature conditions during the synthesis for a given *RE* element. For example, reactions at 1100 °C with the loading composition "$RE_6Zn_2Sb_{14}$" beyond *RE* = Sm, Gd−Ho resulted in admixtures of other phases. For the earlier *RE* elements (*RE* = La, Pr, Nd), the major product was a $Pr_{12}Ga_4Sb_{23}$-type phase.[41] For the later *RE* elements (*RE* = Er, Tm, Lu), only binary *RE*Sb (NaCl-type) and ZnSb (CdSb-type) phases were found. For the divalent *RE* elements (*RE* = Eu, Yb), only binary $RESb_2$, ZnSb (CdSb-type), and unreacted Sb were found. Size and electronic factors are thus important considerations in understanding the stability of the $RE_6Zn_{1+x}Sb_{14+y}$ series.

As described below, the nonstoichiometric nature of this series arises from partial occupancy of Zn sites, as well as possible disorder of Sb sites. In principle, then, there may be a phase width associated with variable Zn or Sb content. The syntheses reported here and elsewhere have been conducted with an excess of Zn relative to the compositions determined from the structure refinements. These refined compositions, ranging from $Pr_6Zn_{1.22(4)}Sb_{14.59(3)}$ to $Ho_6Zn_{1.13(3)}Sb_{14}$, should thus correspond to the maximum Zn content in the phase width for a given *RE* member, but even here there is still some ambiguity. For example, crystals of the Ho compound obtained from our two separate laboratories were prepared from the same loading composition, "$Ho_6Zn_2Sb_{14}$", with different ramping rates to nearly the same annealing temperature (1050 or 1100 °C over 96 h). A faster ramping rate (85 °C/h) led to a lower refined Zn content ($Ho_6Zn_{1.13(3)}Sb_{14}$) whereas a slower ramping rate (25 °C/h) led to a higher refined Zn content ($Ho_6Zn_{1.35(6)}Sb_{14}$). With the caveat that standard uncertainties in refined occupancies are probably underestimated, this observation would be consistent with the relative ease of volatilization of Zn, which possesses a significant vapor pressure at these high temperatures, away from the charge end of the reaction container if the ramping rate is fast. Of the two possible Zn sites, the square pyramidal one (Zn1) exhibits consistently

(41) Mills, A. M.; Mar, A. *Inorg. Chem.* **2000**, *39*, 4599–4607.

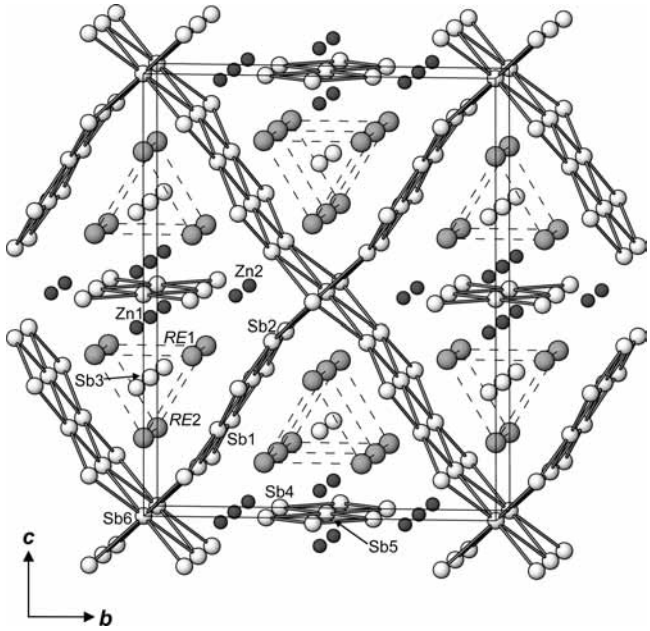

Figure 2. Structure of $RE_6Zn_{1+x}Sb_{14}$ (RE = Sm, Gd−Ho) viewed down the a direction. The large gray spheres are RE atoms, the small solid spheres are Zn atoms, and the medium lightly shaded spheres are Sb atoms. The dashed lines outline the RE_6 trigonal prisms.

lower occupancy (less than 10%) and appears to be most susceptible to depletion, to the extent that it may become effectively vacant. Further work is necessary to understand these synthetic influences before a phase width (which may well differ depending on the RE) can be definitively established, but it is clear that the overall Zn content is higher than previously reported for La_6ZnSb_{15}, where the Zn occupancy was not refined but simply fixed.[30] In subsequent discussion, the formula $RE_6Zn_{1+x}Sb_{14+y}$ will be taken to refer to a general member of the entire series (RE = Pr, Sm, Gd−Ho) or to emphasize the Pr member (where y is ∼0.6), whereas the formula $RE_6Zn_{1+x}Sb_{14}$ is restricted to the Sm and Gd−Ho members (where y is essentially zero).

Crystal Structure and Bonding. Although the structure of $RE_6Zn_{1+x}Sb_{14}$ (RE = Sm, Gd−Ho) is quite complex and strong bonding really extends in three dimensions (Figure 2), it is helpful to decompose it into characteristic fragments. Such an approach not only facilitates the development of structural relationships, but also forms the basis of a "retrotheoretical analysis" for understanding the electronic structure of these and related ternary rare-earth antimonides.[31] For concreteness (useful when bond lengths are discussed), the Gd member is chosen as a representative example of this late RE series. In $Gd_6Zn_{1.5}Sb_{14}$, large 20-membered lozenge-shaped channels extending down the a direction are outlined by Sb atoms forming a polyanionic network, built up of four-atom-wide Sb ribbons or strips (Sb2−Sb1−Sb1−Sb2) on the sides (parallel to (011) and (01$\bar{1}$)) which are linked together by single Sb6 atoms at the corners. These large channels are divided by three-atom-wide Sb ribbons (Sb4−Sb5−Sb4) into two smaller triangular channels, within which lie columns of confacial trigonal prisms with Gd atoms at the vertices and single Sb3 atoms at the centers. The Zn atoms then partially occupy two types of interstitial sites with either square pyramidal (Zn1 (CN5)) or tetrahedral geometry (Zn2 (CN4)).

This description in terms of interstitial Zn atoms occupying a host structure containing a polyanionic Sb network draws attention to related structures, which evolve depending on the RE (Figure 3). Indeed, such a host structure is manifested in the $(U_{0.5}Ho_{0.5})_3Sb_7$ structure type (Figure 3d), adopted by the pseudobinary uranium rare-earth antimonides $(U_{0.5}RE_{0.5})_3Sb_7$ (RE = Y, Gd−Ho).[34] The parent $(U_{0.5}Ho_{0.5})_3Sb_7$ compound itself is probably not amenable to insertion of additional atoms such as Zn, because the two types of interstitial sites are somewhat too small to support reasonable Zn−Sb bonds: the square pyramidal site at 4j (1/2, 0, ∼0.44) would be 2.3−2.6 Å and the tetrahedral site at 4h (0, ∼0.26, 1/2) would be 2.2−2.5 Å distant to the surrounding Sb atoms. Partial filling of these sites in $Gd_6Zn_{1.5}Sb_{14}$ (Figure 3c) is associated with a general expansion of the structure, as seen in its larger cell parameters relative to those in $(U_{0.5}RE_{0.5})_3Sb_7$. The previously reported RE_6ZnSb_{15} series (which forms for the early RE metals as in La_6ZnSb_{15})[30] differs from the $RE_6Zn_{1+x}Sb_{14}$ series (for late RE) in that there are now Sb−Sb pairs instead of single Sb atoms linking the four-atom-wide Sb ribbons together in the polyanionic network (Figure 3a). Only the tetrahedral sites are filled with Zn atoms in La_6ZnSb_{15}, at a partial occupancy fixed at 0.50. (There is evidence to suggest that these occupancies may be variable, as found in the corresponding Mn compounds.[30]) Intermediate between the La- and Gd-containing compounds, $Pr_6Zn_{1.2}Sb_{14.6}$ exhibits a disordered structure in which both Sb−Sb pairs and single Sb atoms can act as the linking nodes, while the Zn atoms occupy both square pyramidal and tetrahedral sites (Figure 3b). Table 4 summarizes the evolution of these structures in terms of the composition of the polyanionic Sb network and the occupation of interstitial Zn sites. Further relationships can be developed with the recently reported compounds Ce_6ZnBi_{14} and Pr_6InSb_{15}, and the interested reader is directed elsewhere for details on the effects of substituting Sb with Bi, or Zn with In.[42] Similar assemblies of these polyanionic networks can be found in other antimonides such as $RE_6Ge_{5-x}Sb_{11+x}$,[43,44] $RE_{12}Ga_4Sb_{23}$,[10,41] and $La_{12}Ga_{3.5}Mn_{0.5}Sb_{23.5}$.[45]

The notion of Zn interstitials entering a rigid host structure fixed by other demands can also be seen in the variation in Zn−Sb distances. Typically, such strongly covalent interactions tend to remain relatively constant within a series even when substitution with a smaller RE tends to contract the structure; for example, the Zn−Sb distances within tetrahedral Zn sites in $REZn_{1-x}Sb_2$ (RE = La−Nd, Sm, Gd, Tb) do not stray beyond the range 2.71−2.73 Å within the entire series.[29] In contrast, the Zn−Sb distances within the tetrahedral Zn2 sites decrease from 2.565(2)−2.717(2) Å in La_6ZnSb_{15}, to 2.512(3)−2.674(3) Å in $Pr_6Zn_{1.2}Sb_{14.6}$, to 2.480(2)−2.648(2) Å in $Gd_6Zn_{1.5}Sb_{14}$ (Figure 4), which can

(42) Tkachuk, A. V.; Tam, T.; Mar, A. *Chem. Met. Alloys* **2008**, *1*, 76–83.
(43) Lam, R.; McDonald, R.; Mar, A. *Inorg. Chem.* **2001**, *40*, 952–959.
(44) Deakin, L.; Lam, R.; Mar, A. *Inorg. Chem.* **2001**, *40*, 960–965.
(45) Crerar, S. J.; Morgan, M. G.; Mar, A. *J. Solid State Chem.* **2003**, *171*, 137–142.

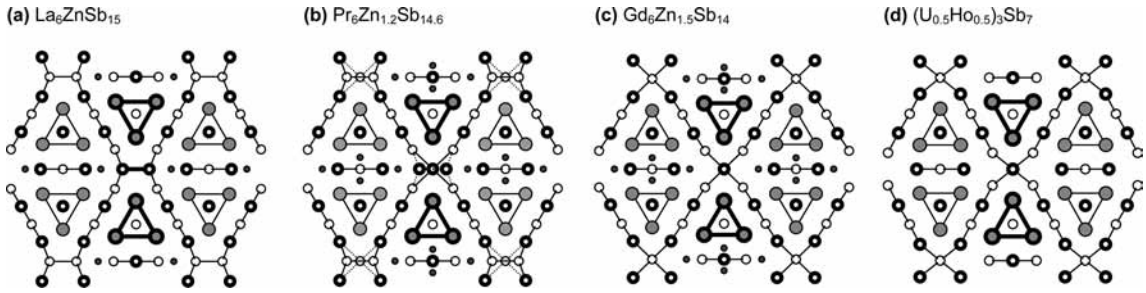

Figure 3. Structures viewed in projection down the shortest axis of ternary rare-earth zinc antimonides for three representative members (a) La_6ZnSb_{15}, (b) $Pr_6Zn_{1.2}Sb_{14.6}$, and (c) $Gd_6Zn_{1.5}Sb_{14}$ derived by filling interstitial Zn sites within the host structure of (d) $(U_{0.5}Ho_{0.5})_3Sb_7$. The large lightly shaded circles are *RE* atoms, the small solid circles are Zn sites, and the medium open circles are Sb atoms. Circles with thicker rims indicate atoms located in planes displaced by half the short axis parameter.

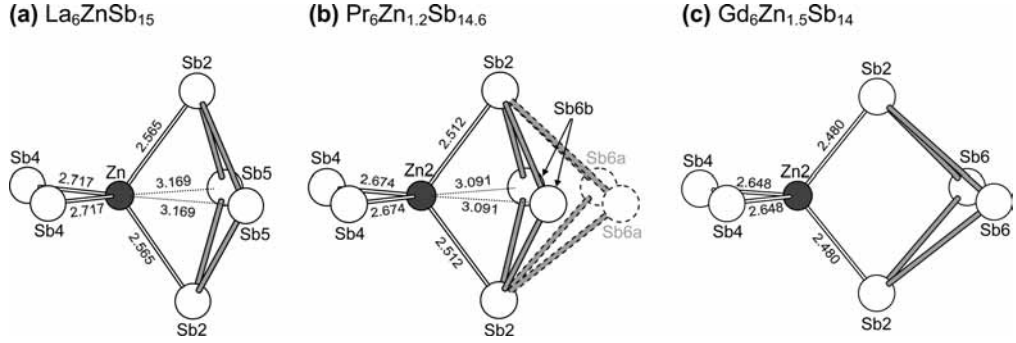

Figure 4. Coordination environment around tetrahedral Zn sites in (a) La_6ZnSb_{15}, (b) $Pr_6Zn_{1.2}Sb_{14.6}$, and (c) $Gd_6Zn_{1.5}Sb_{14}$. Bond distances are in Å.

Table 4. Structural Relationships Between $(U_{0.5}Ho_{0.5})_3Sb_7$ and $RE_6Zn_{1+x}Sb_{14+y}$ (RE = La, Pr, Gd)

compound	$4 \times (U_{0.5}Ho_{0.5})_3Sb_7 = (U_{0.5}Ho_{0.5})_{12}Sb_{28}$	$2 \times La_6ZnSb_{15} = La_{12}Zn_2Sb_{30}$	$2 \times Pr_6Zn_{1.2}Sb_{14.6} = Pr_{12}Zn_{2.4}Sb_{29.2}$	$2 \times Gd_6Zn_{1.5}Sb_{14} = Gd_{12}Zn_{3.0}Sb_{28}$
trigonal prisms	6 U + 6 Ho	12 La	12 Pr	12 Gd
square pyramidal interstitials (4*j*)			0.12×4 Zn = 0.5 Zn	0.04×4 Zn = 0.2 Zn
tetrahedral interstitials (4*h*)		0.5×4 Zn = 2 Zn	0.48×4 Zn = 1.9 Zn	0.70×4 Zn = 2.8 Zn
four-atom-wide ribbons	16 Sb	16 Sb	16 Sb	16 Sb
three-atom-wide ribbons	6 Sb	6 Sb	6 Sb	6 Sb
Sb−Sb pairs (4*g*)		4 Sb	0.61×4 Sb = 2.5 Sb	
single Sb atoms in network (2*a*)	2 Sb		0.35×2 Sb = 0.7 Sb	2 Sb
single Sb atoms in trigonal prisms (4*j*)	4 Sb	4 Sb	4 Sb	4 Sb

be compared to the sum of the Pauling metallic radii ($r_{Zn} + r_{Sb} = 2.63$ Å)[46] and to distances within Zn-centered tetrahedra in $REZn_{1-x}Sb_2$ and other compounds (e.g., 2.671(2)−2.942(2) Å in $Yb_9Zn_{4+x}Sb_9$; 2.694(1) Å in $YbZn_2Sb_2$).[15,22] This observation suggests that Zn−Sb bonding is not optimal in the tetrahedral Zn2 sites within the $RE_6Zn_{1+x}Sb_{14}$ series and becomes increasingly disfavored upon substitution with smaller *RE* metals. Consistent with this proposal, there is evidence that the Zn2 occupancy gradually diminishes from 0.7 to 0.5 on progressing from the Sm to the Ho member, respectively (Table 2). This Zn site is also shifted away from what has been described as a bicapped tetrahedral or a distorted octahedral coordination (CN4 + 2) for the corresponding Mn site in La_6MnSb_{15}.[30,31] As shown in Figure 4, there is a trend toward a strictly tetrahedral coordination in the Zn-containing compounds, and increasingly so with the later *RE* members, where single Sb6 atoms replace Sb5−Sb5 pairs, as described earlier. The origin for this trend can be traced to the competing demands of *RE*−Sb interactions, discussed later.

The occupancy of the square pyramidal Zn1 sites is considerably lower (0.12 or less) than that of the tetrahedral Zn2 sites and is correlated with a splitting of the Sb5 sites (into Sb5a and Sb5b) within the three-atom-wide Sb ribbons. Possible interpretations of the local ordering are depicted in Figure 5. If the Sb5a sites are occupied, the ribbons consist of regular Sb_4 rhombi with equal Sb4−Sb5a distances of 3.084(1) in $Gd_6Zn_{1.5}Sb_{14}$, compatible with hypervalent Sb−Sb bonding typical of such polyantimonide networks.[3,4,31] However, such a ribbon would not support the local occupation of the Zn1 sites because the resulting Zn1−Sb5a distances of 2.39(2) Å would be too short (Figure 5a). If the Sb5b sites are occupied, one possible scenario is the formation of a distorted ribbon with alternately long and short Sb−Sb bonds (2.816(3) and 3.385(4) Å) in irregular Sb_4 rhombi, similar to what has been proposed for La_6MnSb_{15}.[30,31] Local occupation of the Zn1 sites within such a ribbon is only envisageable if the Zn atom caps a larger Sb_4 rhombus, to give reasonable Zn1−Sb5a and Zn1−Sb5b distances (Figure 5b). Moreover, capping on both sides of a rhombus is prohibited by too short Zn1−Zn1 distances (2.34(6) Å). This situation differs from that in Ce_6ZnBi_{14}, where larger Bi_4 rhombi permit a greater occupation of these square pyramidal Zn sites.[42]

(46) Pauling, L. *The Nature of the Chemical Bond*, 3rd ed.; Cornell University Press: Ithaca, NY, 1960.

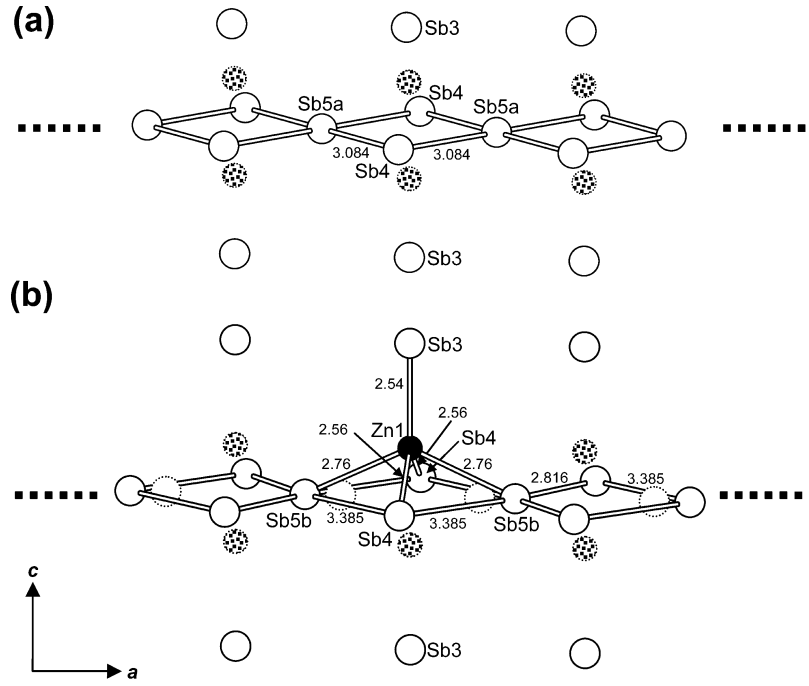

Figure 5. Two possible local ordering arrangements of the partially occupied Zn1, Sb5a, and Sb5b sites within the three-atom-wide Sb ribbons in $RE_6Zn_{1+x}Sb_{14}$: (a) empty Zn1 sites with regular Sb rhombi and (b) partially occupied Zn1 sites with irregular Sb rhombi. Distances shown (in Å) are for $Gd_6Zn_{1.5}Sb_{14}$.

The gradual replacement of Sb−Sb pairs with single Sb atoms as the nodes linking the four-atom-wide Sb ribbons is clearly influenced by the *RE* component. Put simply, this feature can be attributed to lower coordination numbers as the size of the *RE* atom decreases. The structure of $Pr_6Zn_{1.2}Sb_{14.6}$ illustrates these effects well. Around Pr1, the coordination environment of Sb atoms can be described as a monocapped square antiprism (with Sb1−Sb1−Sb1−Sb2 and Sb3−Sb3−Sb4−Sb4 squares) or a tricapped trigonal prism (with eclipsed Sb1−Sb3−Sb4 triangles) (CN9) (Figure 6a), with a relatively narrow range of Pr1−Sb distances (3.2402(7)−3.4001(12) Å) in good agreement with other compounds (e.g., 3.2436(5)−3.3048(6) Å in $PrZn_{0.6}Sb_2$).[29] Around Pr2, however, the coordination environment can be CN10 if the Sb6b sites are occupied or CN9 if the Sb6a sites are occupied (Figure 6b). The Pr2−Sb6b distances are quite long (3.618(1) Å) but are needed to maintain the Sb6b−Sb6b distance no less than ∼2.8 Å, consistent with a single Sb−Sb bond. The Pr2−Sb6a distance is more reasonable (3.337(1) Å) but then the Sb2−Sb6a distances become too long for significant Sb−Sb bonding. The disordered structure of $Pr_6Zn_{1.2}Sb_{14.6}$ thus manifests the transition from La_6ZnSb_{15}, where larger *RE* atoms support optimal bonding around the *RE*2 coordination environment, to $Gd_6Zn_{1.5}Sb_{14}$, where the smaller *RE* atoms force the merging of the Sb−Sb pairs into single Sb atoms.

A full bonding analysis has been performed previously for the closely related La_6MnSb_{15} structure through extended Hückel calculations.[31] An important result of this analysis has been the recognition of antimonide substructures as characteristic building blocks that can be considered independently in formulating the overall electronic structure.[3,4] Remarkably, a Zintl−Klemm approach toward electron counting provides a reasonable explanation for the bonding,

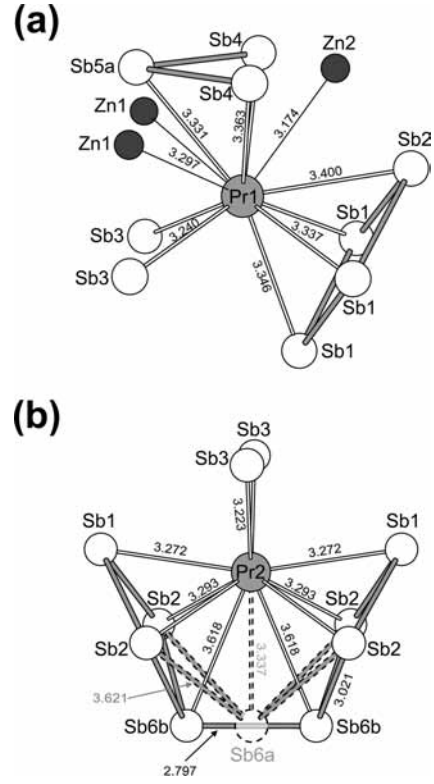

Figure 6. Coordination environment around (a) Pr1 and (b) Pr2 in $Pr_6Zn_{1.2}Sb_{14.6}$. Bond distances are in Å.

even though charge transfer is expected to be minimal given the small differences in electronegativities of the component elements (e.g., the Pauling electronegativities are 1.2 for Gd, 1.6 for Zn, and 2.0 for Sb).[46]If such a simplified analysis is applied to $Gd_6Zn_{1.5}Sb_{14}$, with charges of Gd^{3+} and Zn^{2+} being invoked (these turn out to be consistent with the magnetic measurements (vide infra)), the overall positive

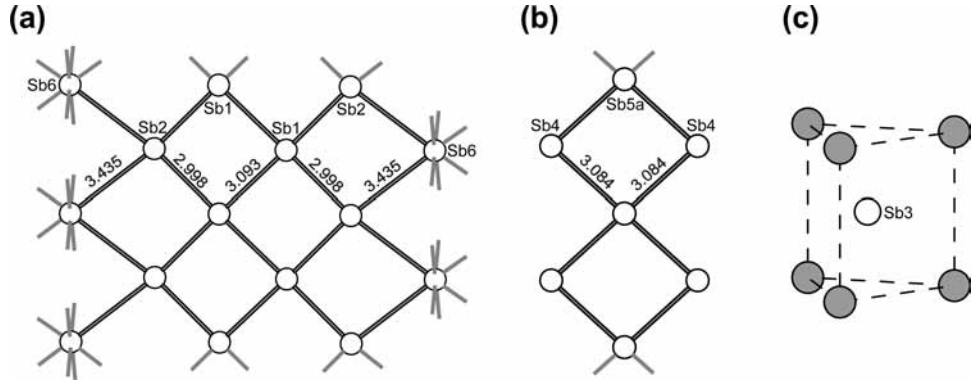

Figure 7. Antimonide substructures in $Gd_6Zn_{1.5}Sb_{14}$: (a) four-atom-wide ribbon, linked to similar ribbons by single Sb atoms, (b) three-atom-wide ribbon, and (c) single Sb atoms centered within Gd_6 trigonal prisms. Bond distances are in Å.

charge of 21+ per formula unit must be compensated by an equal negative charge on the antimonide substructure. Within the three types of antimonide substructures present in $Gd_6Zn_{1.5}Sb_{14}$ (Figure 7), charges on each of the crystallographically inequivalent Sb atoms can be assigned based on the assumptions that the long Sb−Sb contacts are considered to be "one-electron" bonds and that octets are completed with additional lone pairs, if needed. Thus, the four-bonded Sb1, Sb2, and Sb5a atoms are assigned to be 1−, the two-bonded Sb atoms are 2−, and the isolated Sb3 atoms are 3−. The eight-bonded Sb6 atoms are somewhat problematic but they can be estimated to be neutral. The overall negative charge of 19− per formula unit falls two electrons short to satisfy charge balance. Because of the great variability in Sb−Sb distances (d_{ij}), an alternative approach, first proposed by Jeitschko and co-workers, can be taken in which bond valence calculations are applied to these antimonide substructures to yield non-integral formal charges on the Sb atoms.[47,48] If the bond valence parameter R_{ij} for Sb−Sb interactions is set to 2.80 Å and bond valences are calculated through the equation $\nu_{ij} = \exp[(R_{ij} - d_{ij})/0.37]$,[49,50] the charges are found to be 0.9− for Sb1, 1.5− for Sb2, 3− for Sb3, 2.1− for Sb4, 1.1− for Sb5 and 1.6− for Sb6, giving an overall negative charge of 22− per formula unit in $Gd_6Zn_{1.5}Sb_{14}$. Although this result now gives an overestimation of the negative charge, it does reveal the role of these antimonide substructures as electronic sinks, capable of undergoing reduction or oxidation without great cost in energy, as was confirmed in the case of La_6MnSb_{15}.[31] Indeed, the density of states near the Fermi level in these types of compounds typically consists of major contributions from the antimonide substructures, accounting for their usual metallic conductivity.

Magnetic Properties. Magnetic susceptibilities have been measured for $RE_6Zn_{1+x}Sb_{14}$ (RE = Sm, Gd−Ho) from 2 to 300 K under an applied field of 5000 Oe. The plots of χ_m vs T reveal maxima at low temperatures that suggest the onset of long-range antiferromagnetic ordering for the RE = Sm, Tb, Dy, and Ho members, with Néel temperatures of T_N = 6.8, 22.1, 6.3, and 8.9 K, respectively (Figure 8a). In contrast, the Gd member shows no maximum in the magnetic susceptibility down to 2 K. The linear portions of the inverse magnetic susceptibility over the entire temperature range for the Gd member and above T_N in the paramagnetic regime for the Tb, Dy, and Ho members (Figure 8b) can be fit to the Curie−Weiss law, $\chi_m = C/(T - \theta)$. The Curie constants are C = 101, 151, 169, and 167 $cm^3\ mol^{-1}$ K and the Weiss constants are θ = −31, −32, −6, and −13 K for RE = Gd, Tb, Dy, and Ho, respectively. The effective magnetic moments, obtained from the equation $\mu_{eff} = \sqrt{8C}$, are 8.2 μ_B/Gd, 10.0 μ_B/Tb, 10.6 μ_B/Dy, and 10.6 μ_B/Ho, which agree well with the theoretical values for the isolated ground-state RE^{3+} ions (7.9, 9.7, 10.6, and 10.6 μ_B, respectively) obtained from the equation $\mu_{eff} = g[J(J + 1)]^{1/2}$.[51,52] The inverse magnetic susceptibility for the Sm member is distinctly nonlinear (Figure 8c) and is typical for Sm^{3+}-containing compounds, where spin−orbit coupling splits the ^6H ground term for Sm^{3+}, leading to a temperature dependence of the effective moment from the 4f electrons. In general, these results are comparable to those found earlier for $RE_6Ge_{5-x}Sb_{11+x}$, which also undergo antiferromagnetic ordering at low temperatures and share the common structural feature of one-dimensional columns of face-sharing RE_6 trigonal prisms.[44]

Transport Properties and Electronic Structure. To assess the feasibility of $RE_6Zn_{1+x}Sb_{14}$ as thermoelectric materials, preliminary measurements of their charge transport properties have been made. The present measurements are on unoptimized samples and further work will be necessary to understand how the level of Zn deficiencies affects these properties. The electrical resistivity curves for single crystals with RE = Tb, Dy, and Ho from 300 to 2 K reveal metallic behavior and surprisingly good conductivity ($\rho_{300} = 1 \times 10^2$ $\mu\Omega\cdot$cm) notwithstanding the disordered nature of the structure (Figure 9a). At high temperatures, from 300 to 700 K, the electrical resistivity curve for a cold-pressed pellet of a polycrystalline sample of the Ho member (single-phase

(47) Jeitschko, W.; Altmeyer, R. O.; Schelk, M.; Rodewald, U. C. *Z. Anorg. Allg. Chem.* **2001**, *627*, 1932–1940.
(48) Schmidt, T.; Altmeyer, R. O.; Jeitschko, W. *J. Solid State Chem.* **2003**, *173*, 259–272.
(49) Brown, I. D. In *Structure and Bonding in Crystals*; O'Keeffe, M.; Navrotsky, A., Eds.; Academic Press: New York, 1981; Vol. 2, pp 1−30.
(50) O'Keeffe, M.; Brese, N. E. *J. Am. Chem. Soc.* **1991**, *113*, 3226–3229.
(51) Kahn, O. *Molecular Magnetism*; VCH Publishers: New York, 1993.
(52) van Vleck, J. H. *The Theory of Electric and Magnetic Susceptibilities*; Oxford University Press: Oxford, 1932.

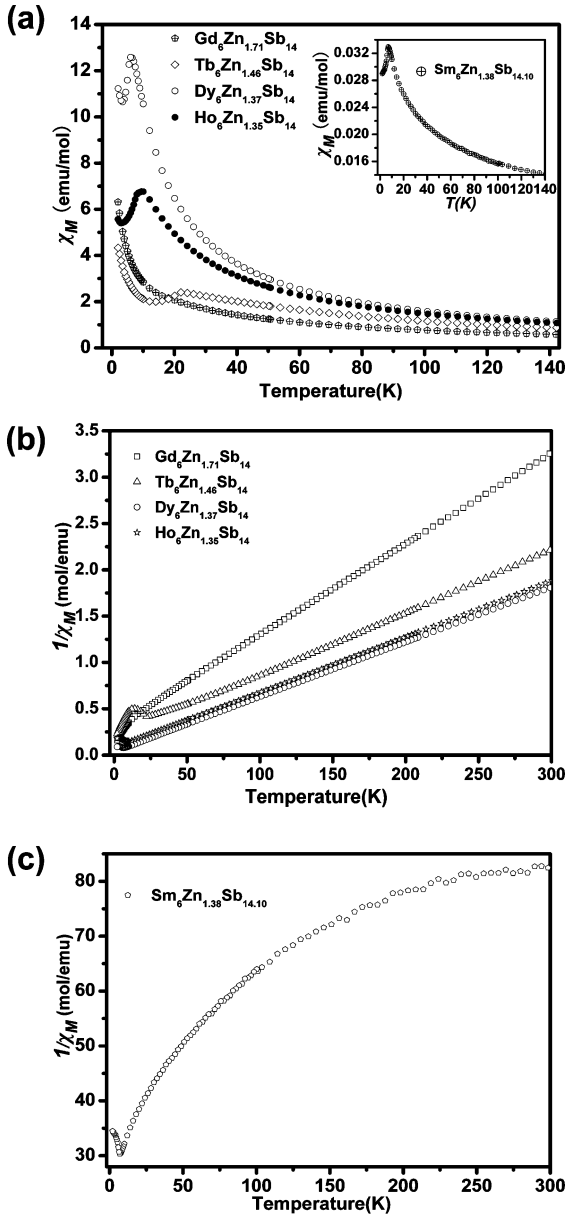

Figure 8. Plots of (a) magnetic susceptibility for $RE_6Zn_{1+x}Sb_{14}$ and inverse magnetic susceptibility for (b) RE = Gd−Ho and (c) Sm.

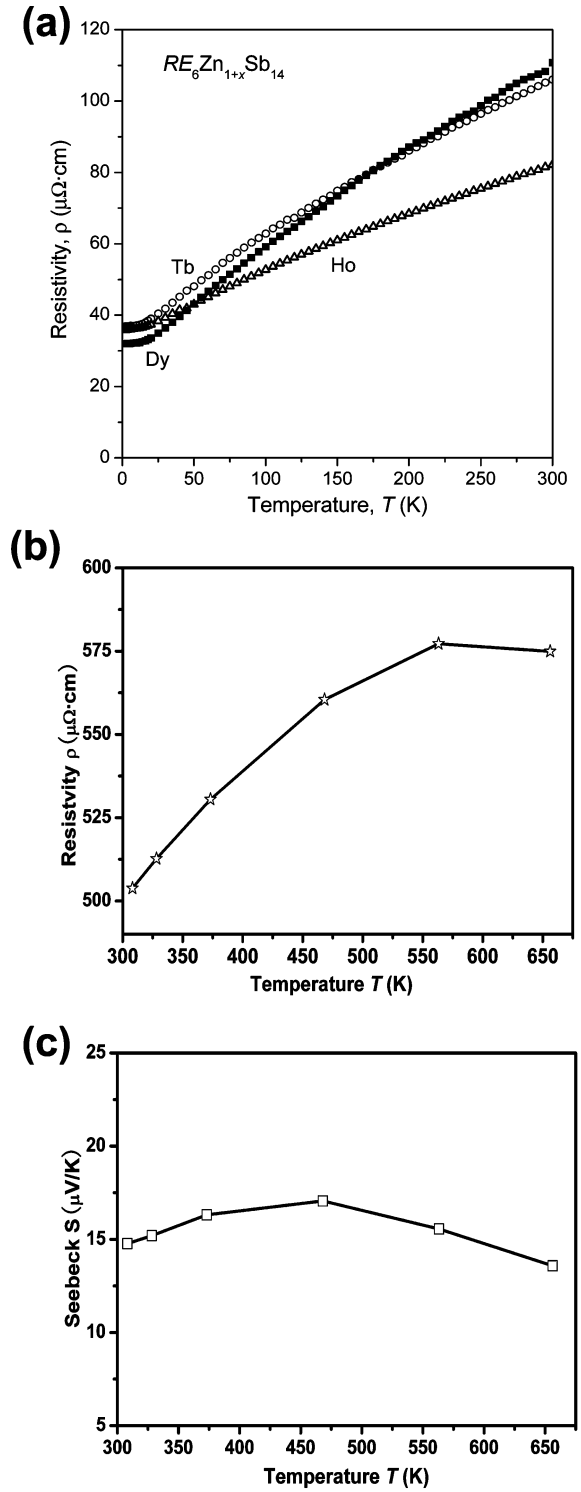

Figure 9. (a) Low-temperature electrical resistivity of $RE_6Zn_{1+x}Sb_{14}$ (RE = Tb, Dy, Ho) single crystals. High-temperature (b) electrical resistivity and (c) Seebeck coefficients of $Ho_6Zn_{1+x}Sb_{14}$ pressed pellet.

according to X-ray diffraction) continues to indicate metallic behavior up to ~600 K (Figure 9b). The absolute values of the resistivity are somewhat higher ($\rho_{300} = 5 \times 10^2\ \mu\Omega\cdot$cm) but consistent with the expected deleterious effect of grain boundaries. Seebeck coefficients measured on the same Ho sample within this temperature range reveal positive values ($S = 15\ \mu$V/K) implying positive charge carriers and small magnitudes consistent with metallic behavior (Figure 9c).

DFT calculations were performed on a hypothetical "$Gd_6Zn_2Sb_{14}$" model, in which the interstitial Zn sites with tetrahedral geometry are fully occupied and those with square pyramidal geometry are empty (Figure 10). The results resemble those found for the closely related structure of La_6MnSb_{15}.[31] The Fermi level falls in a pseudogap, in a region with low density of states (DOS), so that semimetallic behavior is predicted. Below the Fermi level, down to −4 eV, the valence band consists mostly of Gd 5d and Sb 5p states, with a small contribution of Zn 3p states. The real structure is deficient in Zn relative to "$Gd_6Zn_2Sb_{12}$", but the decrease in electron count will only shift the Fermi level negligibly.

Given the presence of many heavy elements (RE and Sb atoms), its complex composition and large unit cell, and the substantial disorder introduced by interstitial Zn atoms, the

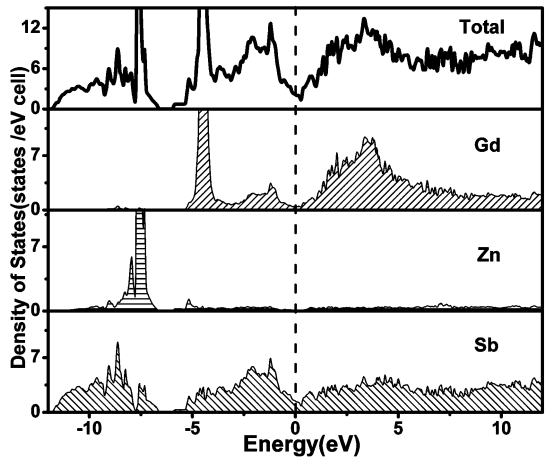

Figure 10. Total and partial density of states (DOS) curves for a hypothetical "$Gd_6Zn_2Sb_{14}$" model. The Fermi level is at 0 eV.

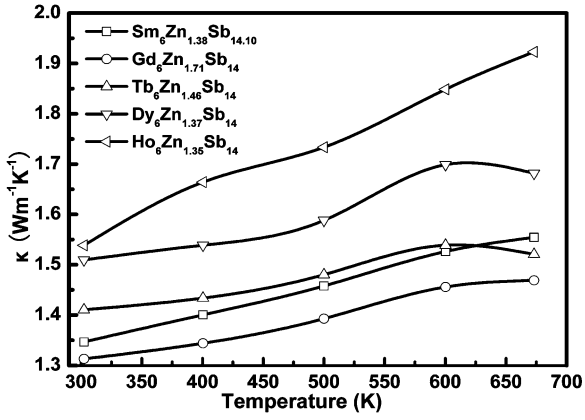

Figure 11. Total thermal conductivity for $RE_6Zn_{1+x}Sb_{14}$ (RE = Sm, Gd−Ho).

$RE_6Zn_{1+x}Sb_{14}$ series may be predicted to display low thermal conductivity, one of the key requirements for a useful thermoelecric material. Figure 11 shows that $RE_6Zn_{1+x}Sb_{14}$ (RE = Sm, Gd−Ho) exhibits rather low thermal conductivities (1.3−1.9 W/m·K between 300 and 675 K), which is comparable to that of optimized Bi_2Te_3 alloy (1.4−1.6 W/m·K). Such low values may be ascribed to the deficiency of Zn.

Conclusion

This investigation has offered not only an interesting illustration of how novel polyantimonide networks remain to be discovered, but also how size effects engendered by the lanthanide contraction act to transform the structure of La_6ZnSb_{15}, where Sb−Sb pairs link the polyantimonide fragments, into that of $RE_6Zn_{1+x}Sb_{14}$ (RE = Sm, Gd−Ho), where the linking nodes are now single Sb atoms. Along this continuum, the critical point is expressed in the intermediate structure of $Pr_6Zn_{1.2}Sb_{14.6}$, in which Sb−Sb pairs and single Sb atoms are disordered. A unifying formula is thus $RE_6Zn_{1+x}Sb_{14+y}$ for the entire RE series. The presence of multiple, partially occupied interstitial Zn sites within an ordered host structure in $RE_6Zn_{1+x}Sb_{14+y}$ is reminiscent of the similar structural features found in "β-Zn_4Sb_3", a recently fashionable candidate for thermoelectric applications.[53] Property measurements on $RE_6Zn_{1+x}Sb_{14}$ reveal that they are generally antiferromagnets with low ordering temperatures, semimetals with reasonably good electrical conductivity, and rather poor thermal conductors. The Seebeck coefficients are, unfortunately, small. Although they are currently not good candidates as thermoelectric materials, appropriate chemical substitution in this series may be worthwhile exploring to improve their properties.

Acknowledgment. The research in China was supported by the National Natural Science Foundation of China (under Projects 20773130, 20521101, 20733003), "Key Project from CAS" (KJCX2-YW-H01, CXJJ-219), "Key Project from FIRSM" (SZD08002), and the Major Programs of Science and Technology Foundation of Fujian Province (2007HZ0005-3). We thank Prof. Li-Dong Chen and Prof. Wen-Qing Zhang in SICCAS for kindly allowing us to use the instruments for thermoelectric property measurements. The work in Canada was supported by the Natural Sciences and Engineering Research Council of Canada and the University of Alberta. We thank Dr. Robert McDonald and Dr. Michael J. Ferguson (X-ray Crystallography Laboratory) for the X-ray data collection and Ms. Christina Barker (Department of Chemical and Materials Engineering) for assistance with the EDX analysis.

Supporting Information Available: X-ray crystallographic files in CIF format. This material is available free of charge via the Internet at http://pubs.acs.org.

IC800524D

(53) Snyder, G. J.; Christensen, M.; Nishibori, E.; Caillat, T.; Iversen, B. B. *Nat. Mater.* **2004**, *3*, 458–463.